CHALLENGES IN THE DEVELOPMENT OF THE
ORBITER RADIATOR SYSTEM

J. L. WILLIAMS
LTV Vought, Dallas, Texas

M. F. MODEST
U. of So. Cal., Los Angeles, California

J. A. OREN
LTV Vought, Dallas, Texas

H. R. HOWELL
LTV Vought, Dallas, Texas

ABSTRACT

This paper describes major technical challenges which were met in the design and development of the Space Shuttle Orbiter Radiator System. This system rejects up to 30 kW of waste heat from eight individual radiators having a combined surface area of $175m^2$. The radiators, which are deployable, are mounted on the inside of the payload bay doors for protection from aerodynamic heating during ascent and re-entry. While in orbit the payload bay doors are opened to expose the radiators for operation. An R21 coolant loop accumulates waste heat from various components in the Orbiter and delivers the heat to the radiators for rejection to space. Specific challenges included high acoustically induced loads during lift-off, severe radiating area constraints, demanding heat load control requirements, and long life goals. Details of major design and analysis efforts are discussed. The success of the developed hardware in satisfying mission objectives showed how well the design challenge was met.

INTRODUCTION

The Space Shuttle Orbiter offered a significant challenge to radiator designers since the high reentry heat flux preludes the use of conventional externally mounted radiators. Mounting the radiators on the inside of the payload bay doors provided a solution to this problem. The doors provide reentry thermal protection to the radiators, and there is no disadvantage associated with having the doors open while the radiators are in operation. This placement solved a difficult problem, but it created several challenges in radiator design which are discussed in this paper. These challenges are primarily related to the radiating area and attachment limitations inherent in the payload bay door mounting scheme, the launch vibration environment, the wide operating temperature range (-130°C to 120°C) and stringent heat transfer and coolant pressure drop constraints. A systems engineering approach was applied universally to design parameters because of the unusually close (for a radiator system) interrelationship of the parameters. The final radiator design will be discussed briefly, and then some of the major challenges associated with the Shuttle Orbiter radiator design will be addressed.

SYSTEM DESCRIPTION

The Orbiter radiator system is described in detail in Reference [1] and flight performance is described in Reference [2]. Briefly the radiator system consists of eight radiators which are evenly divided between two independent Refrigerant 21 (Freon 21) flow loops. Figure 1 shows the routing of one R21
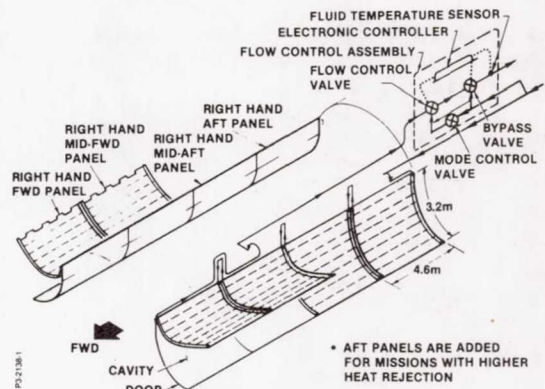

Figure 1 RFCA System Flow Schematic

loop through the four radiators mounted on one side of the payload bay door. Radiator outlet temperature control is achieved by simply bypassing hot R21 around the radiators in the proper quantity such that the mixed temperature of the hot bypassed flow and the cold flow from the radiator is at the desired control point, as shown in Figure 2.
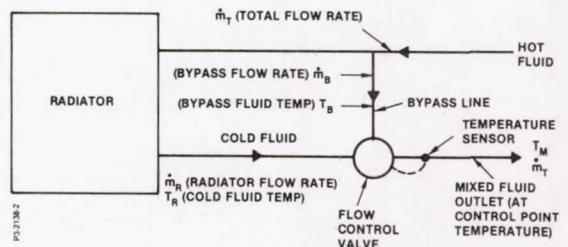

Figure 2 Radiator Temperature Control Approach

The eight radiators are curved to conform to the payload bay doors. Each radiator is about 3.2 m along the curved section by 4.6 m in the longitudinal axis, as shown in Figure 3.
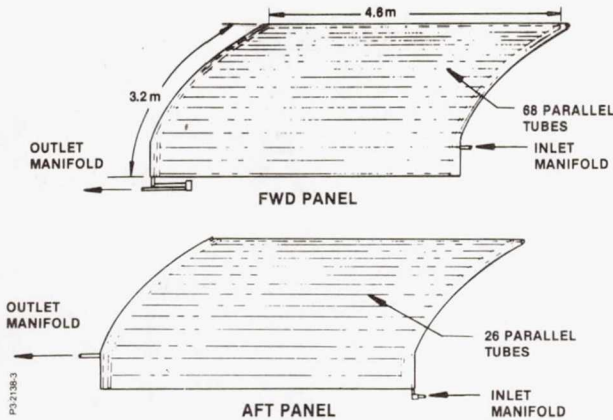

Figure 3 Typical Radiator Panel Physical Characteristics

The forward two radiators, which may be deployed from the door to increase radiator area are each about 2.3 cm thick, while the aft two radiators on each side are about 1.3 cm thick. The radiators are made of bonded aluminum honeycomb structure with tubes attached to the facesheets as shown in Figure 4.
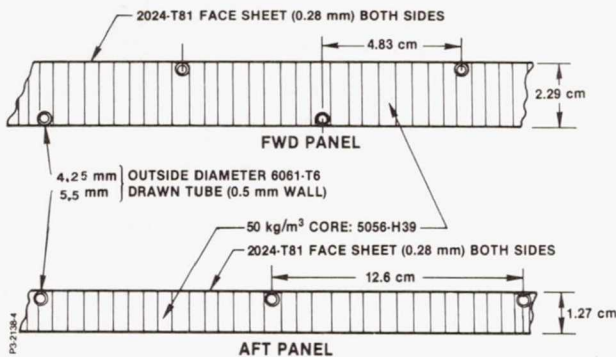

Figure 4 Radiator Panel Honeycomb Layup

HEAT REJECTION OPTIMIZATION

The limited heat transfer area of the inside of the payload bay doors, which represents about 118 sq.m., proved to be inadequate for the required heat rejection of about 20 kW$_t$ in the popular flight attitude of payload bay toward the earth. This made it necessary to deploy the forward radiators away from the doors, as shown in Figure 1, creating a cavity into which additional heat is radiated from the underside of the radiators. Evaluating heat transfer performance gain provided by the cavity was difficult due to the specular silver-backed Teflon surface coating on the

inside of the door and radiators. The radiators had to be optimized for maximum heat radiating efficiency rather than minimum weight and an effective means of applying a long lasting optical solar reflection coating to the radiator had to be devised. These challenges are discussed in the succeeding subsections.

PAYLOAD BAY DOOR-RADIATOR CAVITY ANALYSIS

In order to accurately predict the heat rejection rates from the door-radiator cavity by thermal radiation, radiative exchange factors from surface-to-surface, from surface-to-space, and from sun-to-surface must be determined. The calculation of radiant interchange is commonly performed under the assumption that the participating surfaces are diffuse emitters and diffuse reflectors of radiant energy. Experimental investigations, however, have shown that real surfaces can depart substantially from this model, particularly in the case of smooth and/or metallic surfaces. Extreme examples are deep cavities exposed to incoming radiation (e.g., solar) or outgoing radiation (e.g., heat rejection into space), as are encountered in the Space Shuttle payload bay door-radiator configuration.

Two different methods of calculating radiation exchange factors in complex geometries with complex surface characteristics are possible: the statistical approach (usually called the Monte Carlo method), and the analytic approach, solving a set of simultaneous integral equations numerically. The different approaches require different definitions for the radiative exchange factors. Any numerical method including three-dimensional effects will be complex and computer time-consuming, even if idealized surface properties are assumed. Extremely complex cases such as the payload bay door-radiator cavity with its curved surfaces and its non-ideal surface characteristics are an ideal application for the Monte Carlo technique, which was employed here.

Heat Transfer Relations

Assuming that the door-radiator cavity can be broken up into J isothermal subsurfaces (strips) as shown in Fig. 5, the net heat flux for any strip i may be calculated from

$$Q_i = \int_{A_i} q_i \, dA_i = \epsilon_i \sigma T_i^4 A_i - \sum_{j=1}^{J} \epsilon_j \sigma T_j^4 A_j \mathfrak{F}_{j \to i} - q_{ext} A_s \mathfrak{F}_{s \to i} \qquad [1]$$

$$1 \leqslant i \leqslant J$$

where $\mathfrak{F}_{j \to i}$ = radiative exchange factor from strip j to strip i,

q_{ext} = external energy entering through the opening of the enclosure,

A_s = area of the opening irradiated from external sources,

A_i = strip surface area,

T_i = strip temperature,
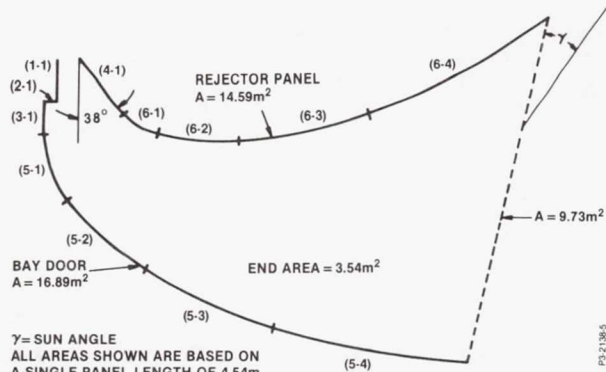
ϵ_i = total hemispherical emissivity of strip.

Figure 5 Bay Door/Rejector Panel Cross Section

REJECTOR PANEL
A = 14.59m²

A = 9.73m²

END AREA = 3.54m²

BAY DOOR
A = 16.89m²

γ = SUN ANGLE
ALL AREAS SHOWN ARE BASED ON
A SINGLE PANEL LENGTH OF 4.54m

Although heat fluxes Q_i can be calculated directly by the Monte Carlo method, it is of advantage to instead determine the exchange factors: although the Q_i's depend on all surface temperatures in the enclosure, the $\mathfrak{I}_{i \to j}$'s either do not (gray surfaces) or depend only on the temperature of the emitting surface (nongray surfaces).

If a large statistical sample of energy bundles N_i is emitted from surface A_i, and if the N_{ij} becomes absorbed by surface A_j after direct travel or after any number of reflections, then the exchange factor may be calculated from

$$\mathfrak{I}_{i \to j} = \lim_{N_i \to \infty} \left(\frac{N_{ij}}{N_i} \right) \cong \left(\frac{N_{ij}}{N_i} \right)_{N_i \gg 1} \qquad [2]$$

Surface Properties.

The accurate calculation of radiation exchange factors requires an extensive knowledge of surface property data. In general, the spectral directional emissivity and absorptivity as well as the bidirectional reflectively must be known for the material for all wavelengths, directions (incoming and/or outgoing solid angles ω), and temperatures; i.e.,

$$\alpha'_\lambda = \epsilon'_\lambda = f(\lambda, \omega, T) \qquad \rho''_\lambda = f(\lambda, \omega_{in}, \omega_{out}, T) \qquad [3]$$

These surface properties must be determined from experiment and/or electromagnetic wave theory. No complete set of surface property data was avilable for silver-backed Teflon, in particular as far as bidirectional reflectivity ρ''_λ is concerned.

For the cavity analysis the following assumptions were made:

1. The properties α'_λ, ϵ'_λ, and ρ''_λ are independent of temperature (this has been shown by experiment to be an accurate assumption for most materials).

2. For infrared wavelengths ($\lambda > 2.5$ μm) and for solar irradiation wavelengths ($\lambda < 2.5$ μm) spectral directional values for emissivity may be calculated from simple correlation formulas, which were based on electromagnetic wave theory combined with available experimental data (an example is shown in Figure 6).
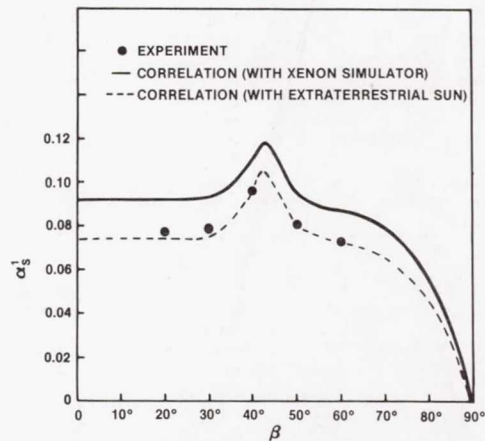

Figure 6 Total Directional Solar Absorptivity of Silver/Teflon

3. The surfaces are smooth and isotropic, so that the bidirectional reflectivity has its maximum in the specular direction and diminishes monotonically for directions farther and farther away.

Surface Description and Ray Tracing

In the computer program all surfaces are described in vectorial form (Reference [3]), where the vector components are polynomials in either one of two perpendicular surface parameters. This description allows for curved or flat "quasi-three-dimensional" surfaces; i.e., surfaces for which there exists a plane such that the projection of the surface on this plane is a (curved or straight) line.

The emission and tracing of energy bundles was carried out by using standard techniques; i.e., by comparing random number with probabilities for emission location, wavelength, and direction, as well as for absorptivities and reflectivities. In order to minimize the required computer time, a number of timesavers were devised, tailored especially to the payload bay door-radiator cavity, which are reported in greater detail elsewhere (Reference [4].)

Results

In order to calculate net heat rejection rates from the deployed panels of the Space Shuttle Orbiter while it is in orbit around the earth, the exchange factors in Eq. (1) must be determined; i. e., the absorbed fractions of (infrared) emission from all subsurfaces and of

482

solar and planetary irradiation entering the cavity through the openings. For comparison with limited experimental data (Reference [5]) the cavity was broken up into a relatively small number of isothermal strips, as shown in Figure 5.

significant self-irradiation, which the experiment neglects.) Not surprisingly, the TRASYS results are also fairly accurate for infrared emission, as the reflectivity of the silver-backed Teflon coating is low in this wavelength range. In the Monte Carlo

Table 1   Radiative Exchange Factors $\mathfrak{F}_{i \to j}$ between Zones of Panel/Door Cavity (Emitting Zone at 80°F)

From strip no. / to		(1-1)	(2-1) + (3-1)	(5-1)	(5-2)	(5-3)	(5-4)	(4-1)	(6-1)	(6-2)	(6-3)	(6-4)
Space												
Experiment (EX)		0.298	0.306	0.421	0.397	0.422	0.481	0.185	0.168	0.245	0.480	0.799
Monte Carlo (MC)		0.295	0.288	0.397	0.414	0.454	0.519	0.184	0.178	0.277	0.495	0.801
TRASYS		0.181	0.421	0.438	0.441	0.473	0.552	0.158	0.210	0.321	0.527	0.819
(1-1)	EX	—	(0.019)^a	(0.013)	(0.015)	(0.013)	(0.009)	0.324	(0.018)	(0.002)	(0.001)	(0.002)
	MC	0.013	0.003	0.008	0.016	0.016	0.011	0.296	0.018	0.000	0.000	0.000
(2-1) + (3-1)	EX	(0.025)	—	(0.043)	(0.036)	(0.020)	(0.012)	0.164	0.090	(0.002)	(0.001)	(0.002)
	MC	0.004	0.191	0.049	0.044	0.024	0.017	0.135	0.077	0.003	0.000	0.000
(5-1)	EX	(0.021)	(0.054)	—	(0.032)	(0.020)	(0.013)	0.217	0.224	(0.042)	(0.002)	(0.003)
	MC	0.017	0.065	0.019	0.018	0.014	0.014	0.202	0.229	0.039	0.003	0.000
(5-2)	EX	(0.037)	(0.068)	(0.049)	—	(0.019)	(0.013)	0.143	0.285	0.180	0.035	(0.003)
	MC	0.041	0.080	0.027	0.010	0.010	0.009	0.126	0.293	0.200	0.031	0.003
(5-3)	EX	(0.045)	(0.053)	(0.042)	(0.027)	—	(0.019)	(0.028)	0.127	0.306	0.170	0.026
	MC	0.060	0.069	0.030	0.012	0.010	0.009	0.027	0.138	0.294	0.179	0.028
(5-4)	EX	(0.045)	(0.045)	(0.039)	(0.026)	(0.026)	—	(0.005)	(0.033)	0.130	0.274	0.139
	MC	0.059	0.060	0.039	0.018	0.013	0.011	0.008	0.031	0.150	0.266	0.154
(4-1)	EX	0.518	0.204	0.214	0.093	(0.013)	(0.002)	—	(0.021)	(0.006)	(0.001)	(0.000)
	MC	0.490	0.162	0.194	0.079	0.011	0.002	0.021	0.003	0.000	0.000	0.000
(6-1)	EX	(0.024)	0.091	0.178	0.151	0.047	(0.009)	(0.017)	—	(0.012)	(0.004)	(0.001)
	MC	0.023	0.081	0.184	0.159	0.050	0.008	0.003	0.012	0.010	0.002	0.000
(6-2)	EX	(0.005)	(0.004)	(0.059)	0.166	0.200	0.061	(0.008)	(0.021)	—	(0.013)	(0.004)
	MC	0.000	0.002	0.053	0.183	0.194	0.072	0.000	0.017	0.013	0.007	0.002
(6-3)	EX	(0.004)	(0.003)	(0.004)	0.048	0.165	0.191	(0.003)	(0.009)	(0.019)	—	(0.007)
	MC	0.000	0.000	0.001	0.045	0.165	0.192	0.000	0.005	0.011	0.010	0.006
(6-4)	EX	(0.010)	(0.007)	(0.007)	(0.005)	0.033	0.129	(0.001)	(0.003)	(0.007)	(0.009)	—
	MC	0.000	0.000	0.000	0.002	0.040	0.138	0.000	0.000	0.004	0.008	0.007
Sum of experiment		1.032	0.854	1.069	0.996	0.978	0.939	1.095	0.999	0.951	0.990	0.986

^{a}Values in parentheses were obtained from TRASYS (Reference [6]).

Table 1 shows a comparison of calculated exchange factors between strips with experimental data. In both cases the emitting strip was assumed (or held) at the constant temperature of 27°C (80°F). The exchange factors from strips to space are the fractions of emitted energy that leave the cavity through all openings, front, rear, and sides. Also included in Table 1 are values for the exchange factors to space as obtained by the TRASYS computer code (Reference [6]), which assumes plane strips with gray, diffuse surface characteristics. In general, the agreement between the experimental exchange factors and the results obtained by the Monte Carlo method is excellent, in spite of the fact that only scarce surface property data were available. Much of the small discrepancies may be attributed to experimental inaccuracies. For small exchange factors the experiment became too unreliable, so the TRASYS data were used. The experimental uncertainty is illustrated by the last row in Table 1, which shows that the sums of the experimental exchange factors do not add up to unity as they should, indicating at least a 10% error margin. (The error is larger in the case of strip (2-1) + (3-1) because of

calculations, an average of about 20,000 energy bundles were traced from each emitting strip. Duplicate runs with different sets of random numbers showed that the results can be assumed accurate to ± 0.005, well within experimental accuracy. With such a tolerance it took approximately 1 min. to calculate the exchange factors from one strip to all strips and openings, using a Univac 1110 computer. This amount of computer time compares favorably with the time used by the less sophisticated TRASYS program, which employs fourth-order integration.

A summary of solar irradiation exchange factors is shown in Figures 7 and 8. In these calculations it is assumed that the sun rays are parallel to the sides of the cavity (i.e., perpendicular to the Shuttle axis) so that all insolation enters through the front openings. The solid lines show exchange factors calculated with absorptivities obtained from the previously discussed correlation and bidirectional reflectivities that direct about 99% of all reflected energy into a cone of 3° half-angle around the specular direction, as indicated by a few experimental data for silver-Teflon. The agreement with experiment is fairly good,

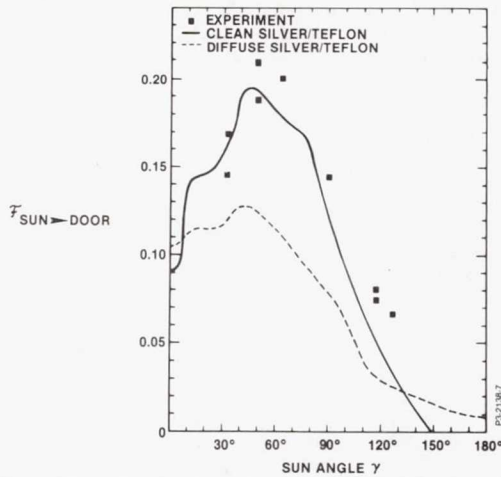especially if one considers that the high

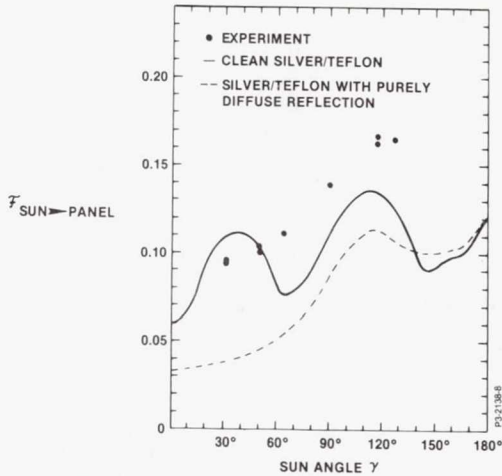Figure 7 Fractions of Incident Solar Flux Absorbed by Bay Door

Figure 8 Fractions of Incident Solar Flux Absorbed by Rejector Panel

reflectivity of the surface ($\sim 90\%$) tends to amplify small inaccuracies in the data for reflectivities and geometry. It is interesting to note what happens to the values of the exchange factors if the surface is a purely specular of a purely diffuse reflector. In the case of purely specular reflection the results practically coincide with the actual reflection pattern, and are therefore not displayed separately. For purely diffuse reflection the absorption rates are reduced, as is the dependence on solar incidence angle. This is shown by the dashed lines. The experimental data seem to follow a diffuse reflection pattern, but with higher absorptivities. This suggests that in the experiment (Reference [5])not enough care was taken to keep the surfaces free of dust or other contaminants, which would tend to increase absorptivity and make reflection more diffuse. In the Monte Carlo calculations about 10,000-20,000 energy bundles were traced for each solar incidence angle. Computer time on the Univac 1110 was again on the average about 1 min. for each incidence angle.

RADIATOR FIN OPTIMIZATION

The radiator panel design is primarily based on design criteria other than thermal. Structural requirements dictate a panel face sheet and honeycomb thickness greater then would be required for weight optimum heat rejection. The coolant loop hydraulic requirements limit the allowable panel pressure drop and hence set the tube size. The only variable available for weight optimizing heat rejection is the tube spacing or number of tubes on the panels. The forward panel (radiation from two sides) tube arrangement also presents an opportunity for optimizing heat rejection. As shown in Figure 4, the tubes on opposite face sheets are staggered to allow heat transfer from the tube through the honeycomb to the opposite face sheet. This effectively increases the radiation fin efficiency by raising the average radiation temperature.

Tube Spacing

The tube spacing or number of tubes on the panel determines the radiation fin effectiveness. As the number of tubes is increased, the fin effectiveness and hence heat rejection are increased but panel weight is also increased. Radiation fin effectiveness of the forward and aft honeycomb layup fin was determined from a two dimensional thermal model which considers heat transfer perpendicular to the tube direction and between the face sheets. The thermal models were verified by element and full scale prototype test data. Figures 9 and 10 show the variation in fin effectiveness with the number of tubes.
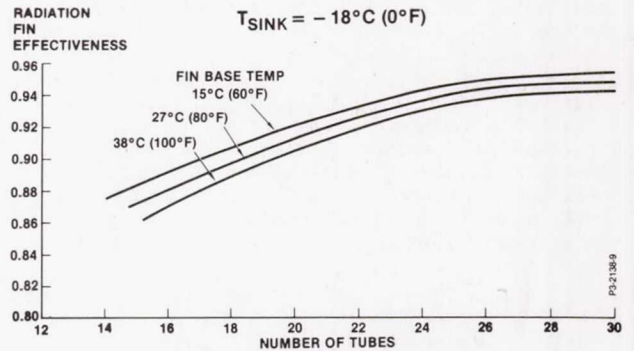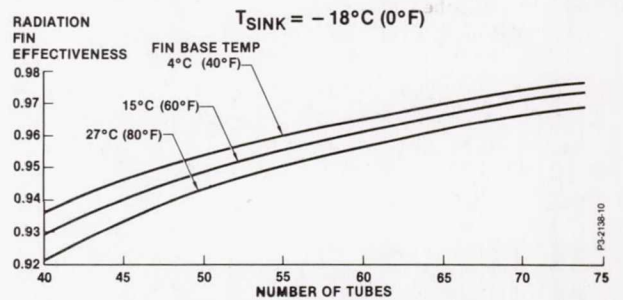

Figure 9 Aft Panel Radiation Fin Effectiveness

Figure 10 Fwd Panel Radiation Fin Effectiveness

484

Tube Size

The radiator tube size is selected to meet the panel pressure drop requirements and to provide a minimum temperature drop between the fluid and the tube. Due to the relatively low thermal conductivity of R-21, the flow must be in the turbulent region to provide adequate heat transfer coefficients. Figure 11 shows the
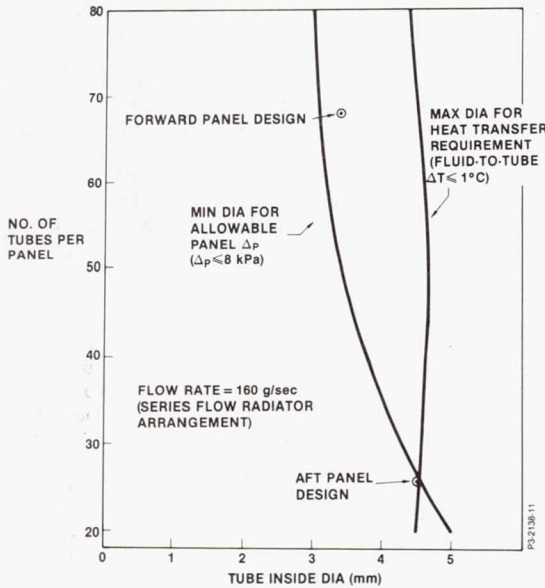

Figure 11 Number of Radiator Tubes versus Allowable Inside Diameter

allowable tube diameters as a function of the number of radiator tubes. A somewhat arbitrary criteria of a $1^{\circ}C$ temperature difference between the fluid and tube is used in this analysis. As indicated, the range of allowable diameters is narrow, and at least 26 tubes are required to meet both the pressure drop and heat transfer criteria. For the heat rejection optimization study a baseline design was established and variations were considered to determine their effect on weight and performance. The relationship between pressure drop, tube diameter and number of tubes is given by:

$$\Delta P = f\left[\frac{w^{1.75}}{D^{4.75}}\right] = f\left[\frac{1}{D^{4.75}}\right]\left[\frac{1}{N^{1.75}}\right] \qquad [4]$$

where ΔP = tube pressure drop
$\quad$ w = tube flow rate
$\quad$ N = number of tubes
$\quad$ D = tube diameter

The fluid to tube area for heat transfer times the convection heat transfer coefficient (hA) is a function of the number of tubes to the 0.2 power and the inverse of the tube diameter to the 0.8 power,

$$hA = f\left[\frac{N^{0.2}}{D^{0.8}}\right] \qquad [5]$$

for turbulent flow. Thus the effect of the number of tubes on hA is found by finding the tube diameter from the pressure drop relationship and the change in hA from the above relationship.

Heat Rejection

A system thermal model that had been verified by correlation with test data was used to optimize the tube spacing. Appropriate fin effectiveness and hA products for various tube spacings were input to the model to determine system heat rejection. Panel weight variations with the number of tubes were used to determine the heat rejection rate per unit weight (BTU/hr-lb). Both 6 panel and 8 panel systems were considered. The heat load and orbital attitudes were chosen such that the heat rejection requirement exceeds the system capacity. This prevents radiator bypass and provides heat rejection optimization under conditions which require maximum radiator performance.
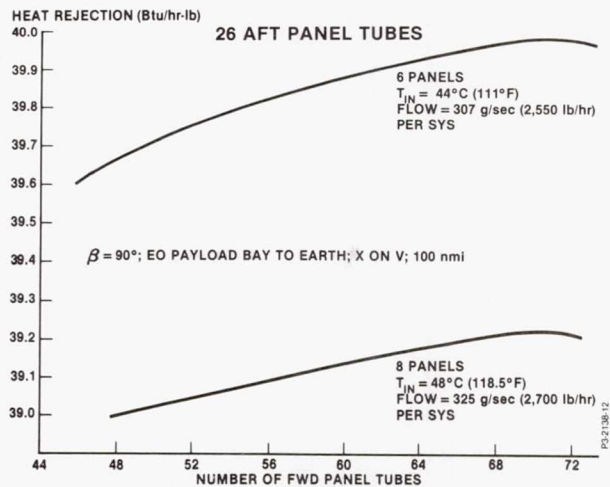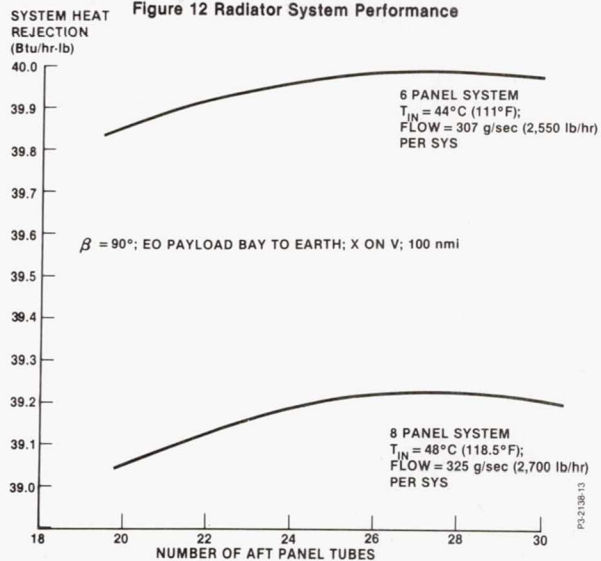

Figure 12 Radiator System Performance

Figure 13 Radiator System Performance

485

Figures 12 and 13 show the system heat rejection per unit weight as a function of the number of tubes on the forward panel and aft panel respectively. It is seen that for both the six panel and eight panel systems the optimum number of forward panel tubes is 70. However, the use of 70 tubes required a non-standard tube inside Diameter of 3.269 mm (0.1287 in). A 68 tube forward panel allows the use of a stock 4.7625 mm OD tube with 0.71 mm wall thickness (3/16 x .028 in) and provides a near optimum design. The cost and schedule aspects of using stock tubing overrides the slight performance gain of the optimum design panel, thus the 68 tube forward panel design was selected.

The aft panel optimization (Figure 13) indicates optimum performance in the range of 26 to 29 tubes. Again, based on the criteria of using stock tubing (6.35 mm OD with 0.889 mm wall thickness) (1/4 X .035 in.) a 26 tube aft panel design was selected. It should be noted that both the forward and aft panel stock tubes are chemically milled to the outer diameters shown on Figure 4 as a weight savings measure.

SYSTEM PERFORMANCE

Performance of the radiator system can be predicted with a high degree of accuracy using large scale computer routines. Results from the foregoing analysis were used to develop a thermal model of the radiator system which includes Orbiter structure with which the radiators interchange energy by thermal radiation. The techniques used and the results of these analyses are reported in detail by Benko (References [7] and [8]) and Howell and Williams (Reference [2]).

Temperature Control

Each of the two R-21 flow loops in the Orbiter contains a Flow Control Assembly (FCA) which performs temperature, fluid flow, pressure drop control and fault detection functions. Incorporating all of these control requirements, some of them quite unusual was a major challenge in hardware design. One such function: temperature control of the coolant is accomplished by simple bypass of the radiators, as shown schematically in Figure 2. Electronic controllers regulate the Flow Control Valve position to maintain the mixed outlet temperature at either 3.3 ± 1^oC or 14.4 ± 1^oC, as selected by the crew. Specifically, the temperature control approach is a closed loop control system with velocity damping. The flow control valve is driven by a stepping motor with approximately 2200 steps from the full radiator flow to full radiator bypass positions. The stepping rate to the valve motor is a function of the temperature error and the rate of change of the temperature error as given by the equation:

$$P = Ge\ Te + Gr\ \frac{d(Te)}{dt} \qquad [6]$$

where P = the pulse rate or stepping rate, pulses/sec.

Ge = The temperature error gain

= 11 Steps/sec-^oC (6 steps/ sec-F) nominally

Gr = The temperature rate of change gain

= 25 Steps/^oC (14 steps/ ^oF nominally

Te = The sensed temperature error

= Tsen-Tset

Tsen = Sensor temperature,

Tset = The set point temperature, 3.3^oC or 14.4^oC (38 ^oF or 57 ^oF) by crew selection

The pulse rate has the limitations of 24 pulses per second maximum and a dead band of zero pulses per second when a pulse rate of less than approximately 1.0 pulses per second is called for. The rate of change term, Gr, was added to the control function when the requirement was imposed to maintain the sensor temperature, Tsen, above the fault temperature of 0.6 ± 0.3^oC (33 ± 0.5^oF) when a rapid decrease in bypass temperature, T_B (see Figure 2) occurs. This rapid decrease in the bypass temperature could be as high as 1.4^oC/sec (2.5^oF/Sec) given by the following relation

$$T_B = T_{BO} - 20\ (1-e^{-t/8}) \qquad [7]$$

where T_B = radiator inlet temperature during downramp, ^oF.

T_{BO} = Radiator inlet temperature at start of downramp, ^oF.

t = time from start of downramp seconds.

This severe transient requirement also imposed restrictions on two other components in the control circuit. The flow control valve was designed to counter the nonlinear variations of the system flow characteristics to provide a linear flow split that is within a band of 15% of full flow and with a local slope of one half to twice the linear slope. In addition the temperature sensor, shown in Figure 2 was required to have a low time constant. The temperature sensor is mounted in a dry well (could be removed without fluid loss) which is filled with thermal grease (Eccotherm TC-4). The resulting time constant has been estimated by correlating test data to be 2.74 seconds for the time constant following a 1.13 second time delay for the fluid temperature change at the control valve to reach the temperature sensor.

There are two valves in each FCA in addition to the Flow Control Valve. The Bypass Valve is plumbed in parallel with the Flow Control Valve with the Bypass Valve in the dominant position. During launch and re-entry the bypass valve is manually activated by the crew to divert flow around the radiator subsystem. The mode control valve is a pre-launch, ground operated hand activated on-off valve which is used to set the pressure drop characteristics of the flow control valve bypass line according to whether six or eight

radiators are being used (to satisfy a requirement that the R21 loop flowrate be lower for eight panels than for six). The pressure drop requirements are shown in Table 2 for the six panel and eight panel system configurations.

TABLE 2 ALLOWABLE FCA PRESSURE DROP

MODE	FLOWRATE g/s(lb/hr)	ΔP ACROSS FCA - kPa(psi) MAX	MIN
6 PNLS	283 (2350)	186 (27.1)	69 (10.0)
6 PNLS	307 (2550)	219 (31.9)	89 (13.0)
8 PNLS	301 (2500)	137 (20.0)	62 (9.1)
8 PNLS	325 (2700)	160 (23.3)	72 (10.4)
BYPASS	331 (2750)	21 (3.0)	-

The Flow Control Valve also required special flow/pressure drop characteristics to meet the system pressure drop needs. Figure 14 shows the valve pressure drop versus valve position designed into the valve by shaping of the poppet to provide the pressure drop control.
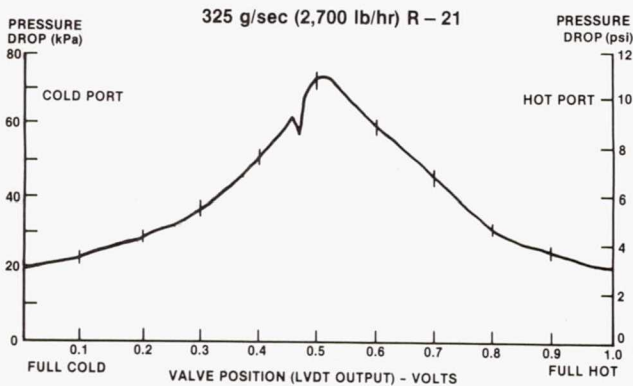

Figure 14 Development Flow Control Valve Acceptance Test Data

The fault detection system on the FCA monitors the temperature of the controlled outlet fluid temperature and automatically switches the bypass valve to full bypass if the temperature goes below 0.6 ± 0.3°C (33 ± 0.5 °F). The FCA also provides for performance monitoring which supplies an electrical signal proportioned to the FCA outlet temperature. The signal is a DC voltage which is zero VDC at −1°C (30°F) and is 5 VDC at 18°C (65°F) The bypass valve positions are also indicated by the performance monitoring system.

FLOW TUBE/STRUCTURE/THERMAL CONTROL COATING INTEGRATION

Thermal control coating selection is a significant challenge for Space Radiators. The desired charactertics for a space radiator coating are high energy emission (low reflectance) in the infrared (or low-temperature) spectrum while being highly reflective in the solar spectrum. The coating also needs to be unaffected by the space environment.

The two general types of coatings used for space radiators are white paints and optical solar reflectors. At the time of the Orbiter radiator development, the optical solar reflector silver-backed Teflon was selected as the best available coating considering thermal performance, maintenance, weight, life, and life cost. A major development program was required to find an adhesive which would satisfactorily bond silver-backed Teflon to structure over the required temperature range of −200°C to 100°C. The selected adhesive was silicone based Permacel 223. An autoclave cure process was developed for using the silver-backed Teflon's P223 adhesive to aluminum. The process will keep P223 bonded to aluminum over a temperature range of −300°C to 120°C in a vacuum.

While thermal studies were showing the need for adhesively bonded silver-backed Teflon, structural analyses were indicating the need for a fatigue resistant structure such as bonded honeycomb. It quickly became apparent that adhesively bonding silver-Teflon to radiators having closely spaced tubes on the outside of the conductive fin, as would be required on the two-sided forward radiators, would be particularly time consuming and conducive to unsatisfactory workmanship. Thus a scheme was developed for embedding the tubes inside the radiator honeycomb layup to provide the smooth surface for silver-Teflon application shown in Figure 4. The smooth exterior surface permits the use of vacum bagging to maintain pressure on the silver-Teflon during the adhesive cure process.

It was found that using conventional raidator tubes with a flange which bonds to the radiator skin was difficult when the tube is embedded in the honeycomb core. Analyses showed that standard round tubes could be used if the bond line between the tube and the skin could be sufficiently reduced and a conductive adhesive was used. A technique was developed for bonding the radiators so the tube-to-skin bond line thickeness would be 0.08 mm or less. This gives a tube to skin temperature drop of 0.5°C, under maximum heat rejection conditions. This compares favorably to other radiator tube-to-fin attachment configurations.

The conductive adhesive, Metlbond 329-7, is loaded with aluminum powder to increase its thermal conductivity. This provides another plus for the radiator honeycomb structure since the aluminum powder loading makes the adhesive's thermal expansion coefficient more nearly match that of aluminum. This permits the structure to operate over a temperature range of −200°C to +175°C without delamination due to thermally induced stresses.

FLUID SYSTEM SEALING

The Orbiter radiator system has a maximum allowable leakage rate of 0.03 scc per second (0.0011 lb/hr). Loss of fluid is to be avoided for the obvious reason that carrying make-up fluid is expensive, and the leaked-out fluid may contaminate other Orbiter systems or payloads. All welded construction was desirable for the Orbiter radiator system to eliminate leakage.

FLANGE JOINTS

Welding was not practical for the connection of the aluminum radiators to the stainless steel flex hoses between radiators as shown in Figure 15. Flange joints were selected
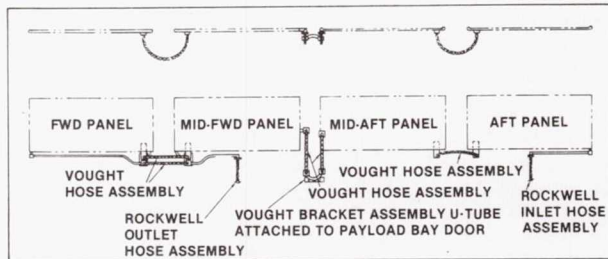
Figure 15 Radiator Interpanel Plumbing

for this joint because effective dissimilar metal corrosion protection is easily provided for them. The aluminum flange is anodized and the stainless steel flange is passivated, and both are coated with super Koropon except on the flange face. When the joint is made, RTV is applied to the interface region.

Obtaining a seal was a more formidible challenge because of the wide temperature range of the radiators (-130°C to 120 °C), and the material compatibility problems associated with R-21. Teflon is the material of choice for R-21 seals; however, it is not satisfactory in O-ring form for the radiator temperature range. Teflon omni-seals were selected because the spring in these seals keeps the seal lips in place over the desired temperature range. In order for the Teflon omni-seal to form a leak-tight seal, it was found that the flange faces should be finished with a tool that has a rotary motion, and that the finish should be in the range of 32-63 -in. RMS. Smoother finishes, or those in which rotary motion of the tool was not used were found to be prone to leak.

MANIFOLD WELDS

The numerous tubes in each radiator are welded into manifolds at each end as shown in Figure 16. The flow tubes are 6061-T6 Aluminum Alloy to provide the yield strength required due to bending of the radiators. Welding of the flow tubes into the manifolds produced "hot short" cracks in the manifolds with all manifold materials and welding techniques tried. Finally a suitable material, Aluminum Alloy 5083, was
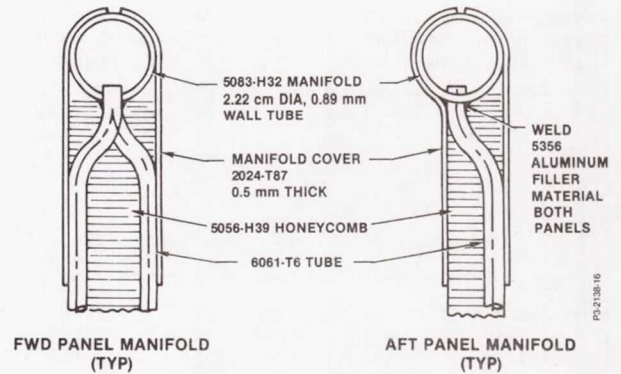
FWD PANEL MANIFOLD (TYP)   **AFT PANEL MANIFOLD (TYP)**

Figure 16 Radiator Manifold Details

found. However, 5083 is not commercially available in seamless tube form. And, while it generally has excellent corrosion characteristics, it is susceptible to stress corrosion if improperly thermally conditioned. Vought bought a billet of 5083 and had it processed into 2.22 cm (7/8-inch) O.D. manifold tubing (Reference [9]). This tubing completely eliminated welding problems throughout the program.

LEAKAGE DETECTION

Proving that leakage of the radiators was within the allowable range was a significant challenge. Halogen detectors are used with great success to verify there is no leakage from the flange joints; however, it is difficult to obtain a quantifiable leakage rate from a large structure such as the radiators with this technique. Vought developed a technique for measuring leakage from an entire radiator. This was done by calibrating a gas Partial Pressure Analyzer reading with a known R21 leak rate within the thermal-vacuum chamber used for radiator acceptance testing (Reference [10]). Most of the radiators have a leakage rate below the minumum detectable level of 10^{-4} scc/sec.

LOADS AND STRESS ANALYSIS

The Orbiter lift-off acoustic noise environment has unusually high energy levels at low frequency; in the 10-20 Hz range in which the large radiators are highly responsive. Determining the loads and stresses on the radiator was a major challenge involving state-of-the-art finite element computer analysis which is beyond the scope of this paper to describe. However, The importance of this challenge was of such magnitude that it must be mentioned in any compilation of Radiator Design Challenges.

Dynamic response models of the entire Orbiter (generated by Rockwell International) were combined with models of the radiators to determine radiator loads. These loads were then used to size radiator structural components. These are reported in References [11] and [12],

and and to very limited extent in Reference (2). The work of Mr. Ron Ott (deceased,1981), was particularly significant in the structural design of the radiator systems.

CONCLUSIONS

The Orbiter radiator system has performed flawlessly as expected during the first six Shuttle flights. During execution of the program all major milestones and all hardware deliveries were met on schedule. In addition, the program was completed under the planned budget. This factor, when considered together with those technical challenges discussed herein, illustrates the extent to which the challenges of Space Shuttle Orbiter Radiator design were satisfied. The well-conceived and executed space radiators research and development programs carried out in the late 1960's and early 1970's provided the basis for the success of the Orbiter Radiator program.

REFERENCES

(1)   Williams, J. L. ; and French, R. J.: Space Shuttle Orbiter Radiator System. Seventh Intersociety Conference on Environmental Systems, ASME paper 77-ENAs-33, 14 July 1977.

(2)   Howell, H. R.; and Williams, J. L. : Qualification of the Space Shuttle Orbiter Radiator System. Eleventh Intersociety Conference on Environmental Systems, SAE Paper 820886, 21 July 1982 (to be published in SAE Proceedings).

(3)   Modest, M. F.; and Poon, S. C.: Determination of Three-Dimensional Radiative Exchange Factors for the Space Shuttle by Monte Carlo; ASME Paper 77-HT-49, 1977.

(4)   Modest, M. F.: Three Dimensional Radiative Exchange Factors for Nongray, Nondiffuse Surfaces. Numerical Heat Transfer, Vol. I, 1978. pp.403-416.

(5)   Scheps, P. B. ; and Howell, H. R.: The Effect of Radiation Trapping within the Cavity Formed by the Shuttle Forward Radiative and Payload Bay Door. ASME paper 76-ENAs-55, 1976.

(6)   Thermal Radiation Analysis System (TRASYS), Martin-Marietta, Contract NAS9-13033, 1973.

(7)   Benko, D. J.: Combined Radiator and Payload Ray Door Thermal Analysis. Vought Report 224RP0100, 22 Dec 1977.

(8)   Benko, D. J.; Postflight Radiator Performance Assessment for STS-4 Mission. Vought Report 2-53200/3DIR-014, 10 May 1983.

(9)   Vought Specification 207-2-407; Tube, Aluminum Alloy, Drawn, Seamless, 5083; 12 Nov. 1976.

(10)   Vought Specification 205-24-019C; Acceptance Test Specification for Radiator Kit, No. 2RH, 11 Nov. 1980.

(11)   Ott, R. E.; Radiator Structural Dynamics Report. Vought Report 224 RP 0113A, 16 March 1981.

(12)   Payne, C. W. ; Space Shuttle Radiator Stress Analysis, Vought Report 224 RP 113 C, 23 Sept. 1981.